ICARUS 82, 180–199 (1989)

Regular Structure in the Inner Cassini Division of Saturn's Rings

BRIAN C. FLYNN

Department of Astronomy, Center for Space Physics, Boston University, Boston, Massachusetts 02215

AND

JEFFREY N. CUZZI

NASA/Ames Research Center, Moffet Field, California 94035

Received October 3, 1988; revised March 14, 1989

Analysis of regular structure in the inner Cassini Division of Saturn has been conducted using Voyager imaging (ISS), radio occultation (RSS), and stellar occultation (PPS) data, with the following results: (1) Virtually identical structure is observed in several Voyager images as was observed in the Voyager 1 RSS scan and identified by E. Marouf and G. Tyler (1986, *Nature* 323, 31–35) as the gravitational wakes of two 10-km-radius satellites orbiting within the division. Results of our analysis of this structure indicate that the regular optical depth variation observed by the RSS scan and the Voyager images is the same structure and that it is essentially azimuthally symmetric. We believe that this rules out the possibility that any large moonlets are responsible for the observed structure. Alternative possible causes of one set of the observed structure are discussed. (2) A comparison of a certain smaller-scale structure observed in the RSS scan with that seen in the same radial region at different longitudes in the Voyager 2 PPS scan may indicate the presence of a small (~1-km-radius) moonlet orbiting within a minor gap of the division.

1. INTRODUCTION

The Cassini Division of Saturn, a 4000-km-wide region of low optical depth separating the A and B Rings, contains several 20- to 40-km-wide, essentially empty gaps which do not have any apparent dynamical cause. Specifically, their lack of association with orbital resonances with major satellites of Saturn suggests that the gaps may be caused by the gravitational influence of a family of embedded moonlets (Lissauer *et al.* 1981, Hénon 1981). Other explanations have also been advanced (Wiesel 1982); however, we will concentrate primarily on the effects of small embedded moonlets on ring structure.

A moonlet embedded in the rings at radius a_s can gravitationally clear a gap that has a width which is related to the mass M_s of the moonlet. The edges of the gap will fall at radii $a_s \pm s$ where the torque by the moonlet on the surrounding ring material, which tends to cause ring material to move away from the moonlet radially, is equal to the viscous torque, which would tend to fill the gap with ring material. Although the theory of gravitational torques ("shepherding") is still incomplete, we may obtain crude estimates for the width $2s$ of a gap which may be cleared by a satellite of given mass M_s by setting the azimuthally averaged viscous torque equal to the azimuthally averaged gravitational torque (Lissauer *et al.* 1981),

$$s = \left(\frac{8G^2}{81\pi\nu a_s\Omega^3}\right)^{1/3} M_s^{2/3}, \qquad (1)$$

where G is the gravitational constant, ν is the kinematic viscosity, and Ω is the orbital

0019-1035/89 $3.00

frequency. More recent work (Borderies *et al.* 1984, Showalter *et al.* 1986) suggests that the shepherding process may be even more efficient, requiring considerably smaller masses. Of course, inferred moonlet radii will only change by the cube root of this difference.

Since the gaps in the Cassini Division all have widths of order 10 km, with the exception of the 250- to 400-km Huygens Gap and the ~200-km "outer rift" (Lissauer *et al.* 1981), simple application of Eq. (1), assuming $\nu \sim 1$ cm^2 sec^{-1} (Lissauer *et al.* 1981), predicts that the moonlets residing in the gaps would have radii of about 2 km, assuming unit density, making direct detection of them in Voyager images difficult. However, it has been demonstrated that an embedded moonlet can create longitudinally extended disturbances in the nearby ring material which are relatively easy to detect (Cuzzi and Scargle 1985, Showalter *et al.* 1986, Marouf *et al.* 1986). The gravitationally induced disturbances, or "wakes," manifest themselves in regular sinusoidal "edge waves" and associated fluctuations in optical depth away from edges. Certain aspects of these perturbations can be used to determine the mass and location of the moonlet.

An embedded moonlet can produce a wavy appearance on the inner and outer edges of the gap containing the moonlet. This wavy edge has an azimuthal wavelength which is proportional to the moonlet's radial distance from the gap edge, and can be approximated by (Cuzzi and Scargle 1985)

$$\lambda_\theta \sim 3\pi s. \tag{2}$$

These patterns are fixed in the frame rotating with the responsible moonlet. Due to differential rotation, the wave pattern on the interior gap edge will lead the moonlet and, likewise, the moonlet will lead the wave pattern on the exterior gap edge. The form of the wavy edge is due to the coherent orbital motion of the particles in elliptical orbits with eccentricity given roughly by

$$e \sim \frac{M_s}{M_p}\left(\frac{a}{a - a_s}\right)^2, \tag{3}$$

where M_p is the mass of the planet and a is the radial location. Since the radial amplitude of the wavy edge is ae, an estimate of M_s may be obtained.

Naturally, these orbital disturbances, which are seen as wavy structure at a gap edge, also occur at a range of radii in the surrounding ring material. However, nothing observable is produced away from the edge until the differential orbital velocities cause the induced oscillations to go out of phase, resulting in regular variations in optical depth emanating away from the gap edge. These optical depth fluctuations may be modeled by

$$\tau(r, \theta) = \frac{\tau_0(a)}{(1 + \mu g(a, a_s, \theta))}, \tag{4}$$

where $\mu = M_s/M_p$, τ_0 is the local mean optical depth, and g is an oscillating function depending only on known geometrical parameters (Showalter *et al.* 1986). Equation (4) can be fitted to the observed optical depth profile, providing another method for estimating the mass of the moonlet M_s.

The wavelength of these variations, or wakes, can be used to determine the moonlet's location. The radial wavelength λ_r at any point in the wake train is roughly given by (Showalter *et al.* 1986)

$$\lambda_r \sim \frac{3\pi a_s \delta^2}{|\theta|}\left(1 - \left|\frac{\delta}{\theta}\right|\tan\alpha\right), \tag{5}$$

where $\delta = (a - a_s)/a_s$, θ is the difference in longitude between the moonlet and the scan, and α is the angle between the radial direction and the scan direction. A fit to the observed pattern provides a location (a_s, θ) for the moonlet.

The methods described above have been applied extensively to the wake seen near the Encke Gap of Saturn, providing strong evidence that an approximately 10-km-radius moonlet orbits close to the center of the gap. More recently, Marouf and Tyler (1986; henceforth MT) have applied these

models to certain structure observed in the Cassini Division by the Voyager Radio Occultation (RSS) experiment, and identified that structure as the wakes of two 10-km-radius moonlets. In this paper, the results of a careful search of Voyager images of this region of the Cassini Division for wake patterns and wavy edges are presented, and the above methods are applied to features found in the division.

Although simple wake theory is not fully understood, as pointed out by all previous authors, its predictions are qualitatively correct regarding wavy edge and wake wavelengths and amplitudes in the case of the Encke Gap. Since it is this simple and effective current version of wake theory which has been used by all prior workers, including MT, to infer moonlets from observed structure, we will, in this paper, continue to apply it to see whether it remains consistent with structure newly analyzed here. The ultimate validity of this simple wake theory is not an issue—only whether it can be applied uniformly well to a diverse set of complementary observations.

The results of our analysis are mixed; first, contrary to the findings of MT, we find that the structure seen in the RSS data is, apparently, azimuthally symmetric; i.e., we see essentially identical structure at a variety of longitudes both close to, and distant from, the locations of the moonlets previously postulated even though the wavelength of a moonlet wake is highly dependent on azimuthal distance from the moonlet (Eq. (5)). In addition, no wavy edges are seen in images obtained at longitudes relative to the MT moonlets where they should not only be detectable but probably easily visible.

Our results do not rule out the presence of similar moonlets at longitudes remote from all of our observations, or of smaller moonlets which may be widely distributed in relative abundance. In Section 3.3, we speculate that some small-scale structure observed by the RSS scan may be the wake of one such smaller moonlet. While this object may be too small to maintain its gap alone, it may be only one of many similar moonlets orbiting there.

2. DATA DESCRIPTION AND REDUCTION

For this study, six high-resolution Voyager images of the Cassini Division were chosen. Of these, two are in transmitted light (views of the unlit face of the rings) and were taken by Voyager 1, and four are in reflected light (views of the lit face) and were taken by Voyager 2. A composite of the four Voyager 2 images (Fig. 1) suggests that two ring edges in the Cassini Division, aside from those of the B Ring and the Huygens Ringlet (Porco 1983), are slightly elliptical while the remainder appear to be circular to within the limits of image resolution. To remove camera pointing errors and place all images in a common radial reference system, all radii in the six images are related to the edge of a ringlet located at a distance of 118,290 km from Saturn (as determined by RSS observations) which appears to have a nonvarying radius in the composite image.

To determine the validity of this choice of benchmark, the uncertainties in the locations of several edge features were calculated from the observed edge locations (defined as the azimuthally averaged radius of the half-power point) in each image and the corresponding radial ring plane resolutions. For the purpose of assigning errors to radial values taken from the images, an average uncertainty for each image was also calculated from the observed edge locations. This uncertainty includes an additional error for the Voyager 1 images since they provide only the brightness of the transmitted light and there is a strongly nonlinear relationship between transmitted brightness and optical depth.

The results of this analysis (see Table I) show that the choice of the ringlet edge at 118,290 km (designated Edge 5; see paragraph on nomenclature below) as a benchmark introduces errors which are within the

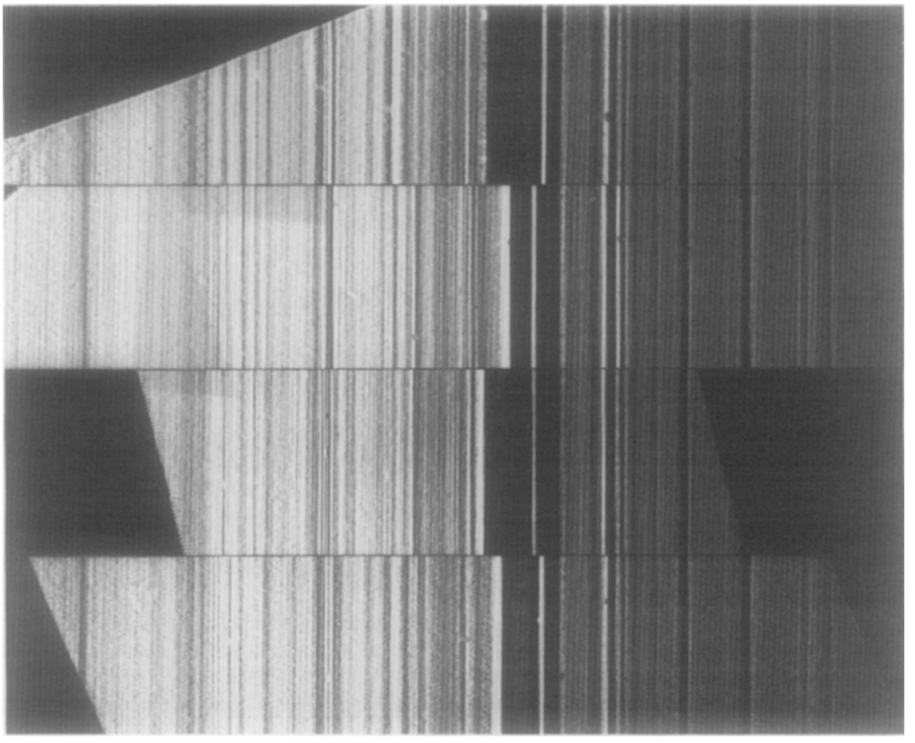

FIG. 1. Composite of four Voyager 2 images of the inner Cassini Division (FDS counts 43989.46, 43993.06, 43994.10, and 43999.37) used in this study. Note the $m = 2$ B Ring edge, the $m = 1$ Huygens Ringlet, and the apparent $m = 1$ edges of Band 1 (reprinted from Smith *et al.* Copyright 1982 by the AAAS).

resolutions of the images, indicating that our approach to correcting for camera pointing errors is successful.

In addition to this image dataset, results of two other Voyager experiments were used in this study. These are the Voyager 1 Radio Science (RSS) radio occultation experiment (Tyler *et al.* 1983) and the Voyager 2 Photopolarimeter (PPS) stellar occultation experiment (Lane *et al.* 1982). The PPS scan is used less extensively in this study due to its relatively high level of noise at the low optical depths which characterize this region of the Cassini Division.

We now establish some conventions of nomenclature for ease of reference. The four main bands in the Cassini Division, with widths of about 300 km and separated by gaps of widths of about 20–40 km, will be referred to as Bands 1 through 4 in order of increasing distance from Saturn (Fig. 2). In addition to these features, there are three narrower ringlets in the division. The innermost of these is the eccentric and optically thick Huygens Ringlet at $1.95R_S$ (Porco 1983) which lies in the Huygens Gap between the outer edge of the B Ring and the inner edge of Band 1. Moving outward, the next is a very faint, narrow, and apparently azimuthally "clumpy" ringlet just interior to the inner edge of Band 1 which will be referred to as R117909, from its mean radius in kilometers. This ringlet can be seen only in the PPS scan or upon close inspection of the high-resolution images referred to in this paper. The third narrow ringlet, which lies between Bands 1 and 2 and is not "clumpy" or "kinky," will be referred to as R118251. Ring edges are numbered 1 through 10 starting with the inner edge of Band 1 and working outward to the outer edge of Band 4. The edges of R118251 are

TABLE I

EDGE LOCATION ANALYSIS

Image (scan)	Edge 1	Edge 2	Edge 3	Edge 4	Edge 5[a]	Edge 7	σ_r[b]	σ_e[c]	σ_t[d]
34931.06	117,939	118,202	118,245	118,275	118,290	118,634	5.7	3.7	9.1
34934.33	117,938	118,200	118,242	118,273	118,290	118,636	4.3	1.8	6.8
43989.46	117,937	118,206	118,240	118,273	118,290	118,637	5.8	1.7	6.0
43993.06	117,936	118,192	118,240	118,267	118,290	118,638	4.7	1.5	4.9
43994.10	117,934	118,202	118,239	118,271	118,290	118,636	4.4	1.4	4.6
43999.37	117,941	118,190	118,241	118,267	118,290	118,639	2.7	1.6	3.1
$\bar{a}$[e]	117,938	118,196	118,241	118,270	118,290	118,637			
Δa[f]	2.5	6.0	1.5	3.0	0.0	1.6			
PPS	117,938	118,187	118,240	118,266	118,290	118,635	1.0		1.0
RSS	117,940	118,189	118,231	118,260	118.290	118,636	1.0		1.0
$\bar{a}$[g]	117,939	118,189	118,236	118,264	118.290	118,636			
Δa[g]	1.4	3.8	4.6	3.8	0.0	1.0			

Note. All values are in kilometers.

[a] Edge 5 is assumed to be located at the RSS value of 118,290 km.

[b] σ_r = radial ring plane resolution.

[c] σ_e = uncertainty for each image introduced from choice of benchmark, calculated from $\sigma_e(i)^2 = (1/M)\ \Sigma_{j=1}^{M}\ (a_{j,i} - \bar{a}_j)^2$, where $a_{j,i}$ is the observed location of each feature $j = 1, M$ (excluding Edges 1 and 2 due to their observed eccentricities) in each image $i = 1, N$.

[d] σ_t = total uncertainty incorporating (a), (b), and uncertainty due to radiative transfer model (applies to images taken in transmitted light).

[e] $\bar{a}$ = mean edge location from $\bar{a}_j = \Sigma_{i=1}^{N}\ (a_{j,i}/\sigma_r(i)_2)/\Sigma_{i=1}^{N}\ (1/\sigma_r(i)^2)$.

[f] Δa = edge location uncertainty from $\Delta a(j)^2 = \Sigma_{i=1}^{N}\ ((a_{j,i} - \bar{a}_j)^2/\sigma_r(i)^2)/\Sigma_{i=1}^{N}\ (1/\sigma_r(i)^2)$,

[g] Including RSS and PPS scans as well as images.

included in this scheme. All other features will be referred to in a manner indicative of their locations.

3. DATA ANALYSIS

3.1. RADIAL STRUCTURE

3.1.1. Radial Structure of Band 1

The six Voyager images, the PPS scan, and the RSS scan were examined for any wake-like features. The PPS and RSS scans are well suited to this because they provide radial optical depth profiles directly in which wake features are easily detected. Unfortunately, the level of noise in the PPS scan of the low-optical-depth Cassini Division is so high that it could not be used for this purpose. The RSS scan, however, reveals quite prominent and regular optical depth fluctuations in Bands 1 and 2 (MT; see Fig. 3). As noted earlier, application of the moonlet wake model to these features implies that the structure in Band 1 is the wake of an approximately 10-km-radius moonlet orbiting between Edges 4 and 5 at about 118,269 km from Saturn, trailing the RSS scan by 14.8°. Similarly, the structure in Band 2 may be ascribed to a moonlet located between Edges 2 and 3 at about 118,213 km, 9.7° ahead of the RSS scan.

In order to examine the Voyager images for wakes, radial brightness scans were generated by azimuthally averaging brightness values over a prespecified range in radius (Fig. 4). These scans reveal that all six images detect some regular structure in Band 1; less obvious, although clearly present, regular structure in Band 2 is seen in two images.

We first consider the structure detected in Band 1. Four of the six images and the RSS scan reveal a pattern with the same

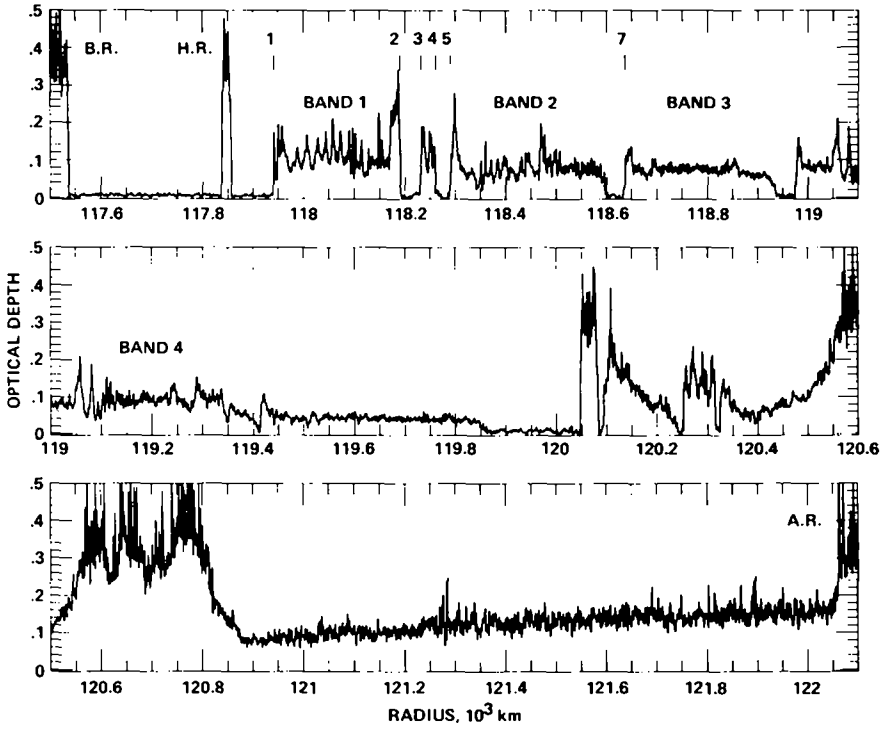

FIG. 2. RSS scan of the entire Cassini Division ranging from the outer edge of the B Ring at a radius of 117,540 km, to the inner edge of the A Ring at 122,050 km. Some features of interest: the Huygens Gap (117,540 km to 117,940 km) which contains the Huygens Ringlet at 117,848 km, Bands 1 through 4, centered at 118,060, 118,440, 118,780, and 119,410 km, respectively, and the Outer Rift ranging from 119,850 to 120,050 km. Edges 1 through 5 and 7 are indicated by integers. The locations of MT's two moonlets are 118,213 and 118,269 km. Optical depth values have been divided by 2 (Cuzzi *et al.* 1984).

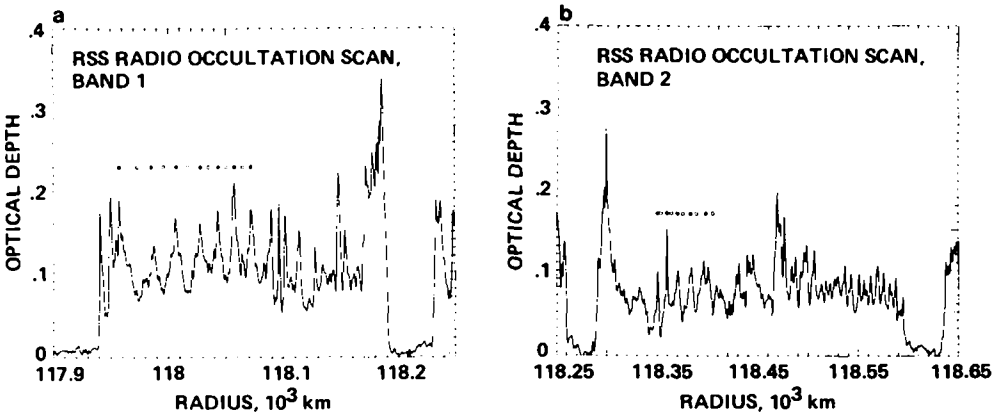

FIG. 3. (a) RSS scan of Band 1 showing region of regular optical depth variation. Optical depth maxima are indicated by closed circles and minima are indicated by open circles. (b) RSS scan of Band 2. The regular fluctuations lie between 118,350 and 118,450 km.

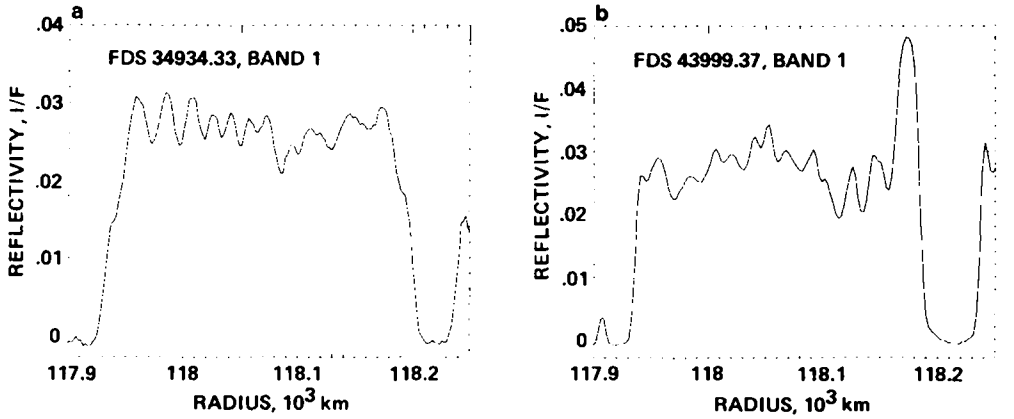

FIG. 4. (a) Brightness scan of Band 1 taken from image FDS 34934.33, showing regular brightness fluctuations. (b) Brightness scan of Band 1 taken from image FDS 43999.37.

number of extrema and with very similar locations (Fig. 5). The images include the two Voyager 1 images (FDS 34931.06, FDS 34934.33) and the Voyager 2 images FDS 43993.06 and FDS 43999.37. Perhaps due to their lower resolution, the remaining two images (FDS 43989.46, FDS 43994.10) have fewer extrema than the other four images and the RSS scan, although they are very similar to each other in terms of numbers of extrema and locations. The general trend of decreasing wavelength with increasing radius is common to all images and the RSS scan. The similarity of Band 1 structure in images FDS 34931.06, FDS 34934.33, FDS 43993.06, and FDS 43999.37 to that of the RSS scan shown by Fig. 5 indicates azimuthal symmetry.

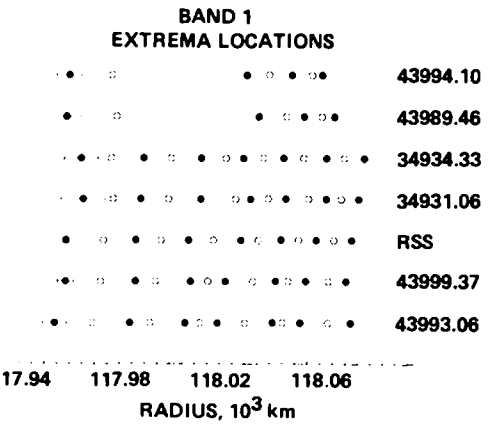

FIG. 5. Plot of all Band 1 extrema locations for images and RSS scan. Closed circles indicate brightness (optical depth) maxima and open circles indicate minima. The vertical ordering is in increasing longitude after precession to the epoch of the RSS scan at the free rate corresponding to the mean centerline radius of Band 1. Typical uncertainties are plotted for one extremum.

The radial structure of wake patterns is highly dependent on azimuthal distance from the responsible moonlet (Showalter *et al.* 1986, MT). If the patterns in the images and the RSS profile of Band 1 are all caused by a moonlet orbiting at 118,269 km, the images and the RSS scan, which reveal quite similar structure, must lie very close in longitude in a system which rotates at the orbital rate of the moonlet. Taking into account the oblateness of Saturn, a precise orbital rate Ω_s at orbital radius a_s can be determined from Saturn's mass, equatorial radius, and gravitational moments (Lissauer and Cuzzi 1982). Upon precessing the image longitudes to the epoch of the RSS scan at the rate $\Omega_s = 752.^{\circ}0\ \text{day}^{-1}$, we find that only image FDS 43999.37 lies close to the RSS longitude while the other five images are widely distributed (Fig. 6), which makes the possibility that they are all caused by a single moonlet orbiting at

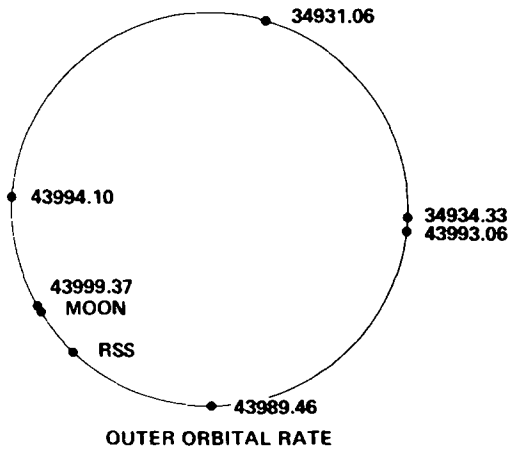

FIG. 6. Image locations after precession to Spacecraft Event Time (SCET) of RSS scan (1980 318.2046225694) at orbital rate of MT outer moonlet (752°0 day^{-1}). The direction of orbital motion is counterclockwise.

118,269 km extremely unlikely. In addition, the close proximity of image FDS 43999.37 ($\theta_s - 2° \pm 30$)[1] to the predicted location of the outer moonlet should make it a good candidate for strong wavy edges. However, we were unable to detect any wavy edges using the method of Cuzzi and Scargle (1985), in spite of the high resolution of the image (2.7 km/pixel in the radial direction). It should be pointed out that although FDS 43999.37 lies close to the predicted location of the moonlet and RSS scan after precessing, uncertainties in the moonlet's orbital frequency and the large time difference between the two observations could place FDS 43999.37 on either side of the RSS scan. However, the radial location of the structure observed in this image and its trend in wavelength indicate that it would be ahead of the moonlet in longitude (see below), leading one to expect edge waves to be found on Edges 2 through 4, with the greatest amplitudes occurring on Edge 4 (see Section 3.2).

Because the structure in all images is so similar, straightforward application of the moonlet wake model (Eq. (5)) to the Band 1 extrema locations in all six images suggests that each image leads a moonlet by about 15°, i.e., the same difference in longitude as inferred from the RSS scan. This in itself would seem an unlikely coincidence for such a randomly chosen set of observations. Furthermore, if each image were this close to a moonlet, the wavelengths and radial locations of the wake patterns would all vary detectably across the longitudinal extent of the images (with the possible exception of 43999.37; see Table II). In fact, no such variation is seen in any of the six images.

To summarize, virtually identical radial structure is seen in the RSS scan and four of the six images, in spite of the fact that the observations are widely spaced in the frame of a moonlet at the implied orbital radius. This situation is inconsistent with the strong azimuthal variation which is characteristic of the moonlet wake theory. Also,

TABLE II

EXPECTED RADIAL VARIATIONS OF EXTREMA

Image FDS count	$\Delta\theta_i$[a]	θ_s[b]	$\Delta\lambda_r$[c] (km)	σ_r[d] (km)
34931.06	15	15	13.6	5.7
34934.33	11	15	11.5	4.3
43989.46	8	15[e]	9.5	5.8
43993.06	7	15	8.7	4.7
43994.10	5	15[e]	6.8	4.4
43999.37	2	16	3.2	2.7

[a] Coverage in longitude of Band 1 for each image (degrees).

[b] Longitudinal distance from the moonlet inferred from each image using wake model of Eq. (5).

[c] The *expected* change in wavelength of the wake across $\Delta\theta_i$ in the image frame due to the strong dependence of λ_r on θ_s.

[d] Radial ring plane resolution.

[e] Assumes the RSS longitudinal distance from the moonlet since these two images have too low a resolution to display a wake pattern which can be fairly "analyzed."

[1] Due to the absolute error of ~10 km in RSS radii (MT), precessing the Voyager 2 images to the RSS epoch results in an azimuthal uncertainty of ~30°. Precessing the Voyager 1 images to the RSS epoch, which are on the order of a day apart, results in an uncertainty of less than 1°.

all six images are close enough to the moonlet location inferred by application of wake theory to their structure to exhibit variation in wavelength across the image, which is not observed. Finally, the presence and structure of a moonlet wake and the inferred proximity of the responsible moonlet(s) almost necessitate the presence of substantial wavy edges, which are not observed (see Section 3.2). Therefore, we believe that the Band 1 structure discussed in this paper is not due to embedded moonlets at all, but is, essentially, azimuthally symmetric structure observed at different times, longitudes, and viewing geometries.

3.1.2. Photometric Modeling

To demonstrate this in more detail, we apply a standard radiative transfer model to the RSS scan optical depths to obtain predicted values of ring brightness, or I/F, for the illumination and viewing geometry of each image using the appropriate single-scattering albedo and phase function of a typical ring particle (see, e.g., Cuzzi *et al.* 1984, Appendix). This radiative transfer model calculates the brightness due to singly scattered light of a homogeneous layer of well-separated particles with normal optical depth τ.

In applying this model, we used the optical depths observed by the RSS experiment, as scaled for the known wavelength-dependent scattering efficiency of the particles. The scaling factor τ_{vis}/τ_{RSS} was determined using the RSS scan and an optical depth profile taken from Voyager images (Cuzzi *et al.* 1984) by

$$\frac{\tau_{vis}}{\tau_{RSS}} = \frac{1}{N}\sum_{j=1}^{N}\frac{\tau_{vis}(R(j))}{\tau_{RSS}(R(j))}. \qquad (6)$$

Since the two optical depth profiles are of differing resolutions, linear interpolation was used to obtain values of the lower-resolution τ_{vis} profile at appropriate radii. The above ratio was found to be 0.5 for the region of the Cassini Division being considered.

When the optical depth profile of Band 1 obtained from the RSS scan is used to calculate I/F values for the viewing geometries of the four Voyager 2 images, and these values are appropriately smoothed to the resolution of each image, the results strongly resemble the image brightness scans, especially for FDS 43999.37 (Fig. 7) and FDS 43993.06. Small differences in relative amplitude could easily be ascribed to small variations in particle albedo or phase function. Applying this method to the lower-resolution Voyager 2 images FDS 43989.46 and FDS 43994.10 with suitably increased smoothing, we find that the resulting model profiles lose some of the lower-contrast extrema, suggesting that the lower number of extrema observed in these images may be an effect of resolution and viewing geometry. These results further support the hypothesis that the structure in Band 1 is more or less azimuthally symmetric with the profile measured at highest radial resolution by the RSS scan.

Although the locations of *brightness* extrema in the Voyager 1 images FDS 34934.33 and FDS 34931.06 agree well with the RSS *optical depth* extrema, there is poor agreement between the observed contrast of the images and the predictions of

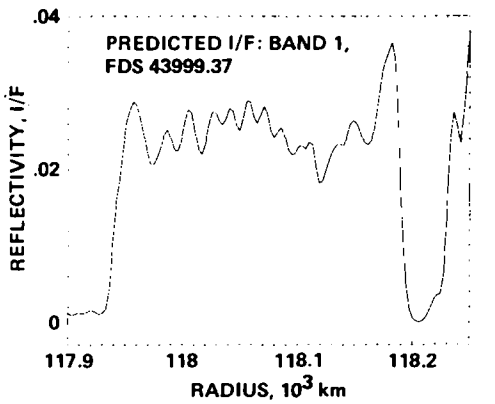

FIG. 7. Standard radiative transfer model prediction of Band 1 brightness profile for viewing geometry of image 43999.37 using optical depths obtained from RSS scan.

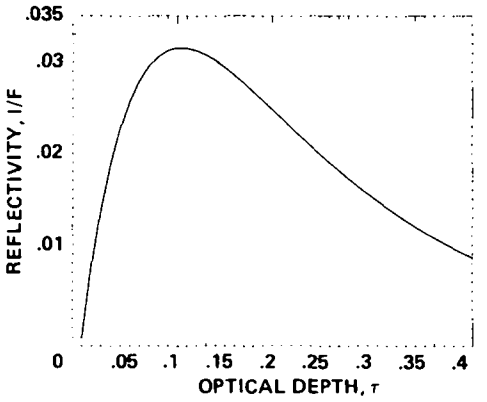

FIG. 8. Predicted dependence of brightness on optical depth for the viewing geometry of image FDS 34934.33.

contrast by the above simple radiative transfer model. It is important to realize that the brightness variation curve predicted for this observing geometry is strongly peaked at a τ close to the average for this region (Fig. 8), and small uncertainties in the scaling factor τ_{vis}/τ_{RSS} can strongly effect not only the contrast, but even the sense, of the brightness extrema. For example, brightness maxima could be either optical depth minima or optical depth maxima, or an even more complicated combination could result. Because the range of τ in Band 1 is so close to the peak of the curve shown in Fig. 8, the predictions of our simple model show almost no contrast at all. In addition, for images FDS 43931.06 and FDS 34934.33, the locations of brightness maxima agree very well with the RSS optical depth maxima locations, and the same is true for brightness minima and optical depth minima. These observations suggest that the peak of the actual brightness–optical depth curve must occur at an optical depth (say $\tau \sim 0.2$) higher than that predicted by our simple radiative transfer model. In this illumination and viewing geometry, model predictions are extremely sensitive not only to the above uncertainties but also to various potential nonideal aspects of the ring vertical structure, such as particle packing effects. Consequently, although we are not able to model these I/F variations in a satisfactory manner we do not think these discrepancies affect our basic conclusions. Future analysis with our improved radiative transfer model (Dones, personal communication 1988) will be of great interest.

3.1.3. Radial Structure of Band 2

In the case of Band 2, the images FDS 43993.06 and FDS 43999.37 clearly show regular radial brightness fluctuations in the range between 118,350 and 118,450 km in radius, while the remaining four images reveal little or no regular structure in this region. The regular structures found in images FDS 43993.06 and FDS 43999.37 occur in the same region of Band 2 and contain approximately the same number of extrema as do the regular optical variations found in the RSS scan (Fig. 9), which may be interpreted as the wake of a moonlet orbiting at a_s = 118,213 km. We note that the shorter-wavelength structure seen in the RSS scan between 118,340 and 118,380 km (Fig. 3b) could easily have been lost due to marginal resolution of the image scan. These similarities, while not as striking as in the case of Band 1, suggest that the type of analysis performed on the regular structure of Band 1 might be relevant in Band 2 as well.

If the Band 2 structure found in the RSS

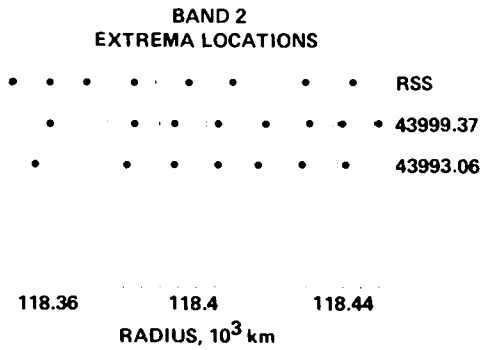

FIG. 9. Same as Fig. 5 except that the extrema locations plotted are for Band 2. Uncertainties are the same as those plotted in Fig. 5.

scan and the images FDS 43993.06 and FDS 43999.37 were caused by a single moonlet, then, after precessing these three observations to a common epoch at the moonlet's orbital rate, we would expect the two images to lie very near *each other* in longitude since their Band 2 structures are virtually identical. In addition, we would expect the two images to lie roughly near the RSS scan because of their crude similarity in average wavelength to the RSS values, and downrange from the moonlet due to the fact that a moonlet wake exterior to a moonlet trails the moonlet in longitude. Figure 10 shows that after precession at the corresponding moonlet orbital rate (a_s = 118,213 km, Ω = 752°.6 day^{-1}), none of the predictions are borne out. While FDS 43993.06 is near the RSS scan and the moonlet, the image FDS 43999.37 falls ~180° ± 30 away.

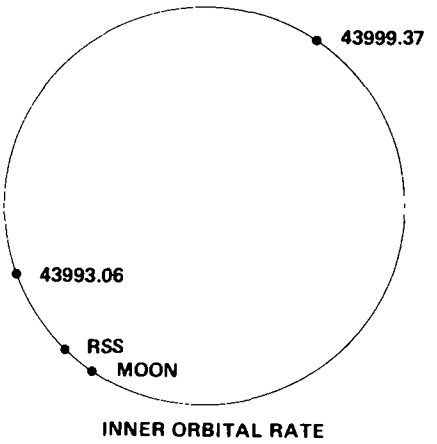

FIG. 10. Same as Fig. 6 except that the MT inner orbital rate was used for precession (752°.6 day^{-1}).

Overall, the similarity of radial structure in the region at the three longitudes and the complete lack of wavy edges in any of the six images (described in detail in Section 3.2) tend to rule out the hypothesis of a single moonlet or moonlets as large as 10 km in radius as the cause of the observed Band 2 structure.

3.2. Azimuthal Structure

Moonlets having the masses inferred from the RSS Band 1 and 2 structure would cause wavy edges with amplitudes *ae* comparable to the widths of the gaps in which they reside, based on simple theory and analogy with the Encke moonlet's observed behavior (Cuzzi and Scargle 1985). To show that this is true, we multiply Eq. (3) by the edge location a to relate the amplitude ae to the moonlet mass M_s. In the case of image FDS 43999.37, if it were trailing the outer RSS moonlet by the distance $\theta \sim$ 15° predicted from wake theory, it would be unlikely for the wavy edges to have damped appreciably. For example, Encke Gap wavy edges with amplitudes in good agreement with current wake theory are easily seen ≈15° away from the moonlet and persist, with decreasing amplitude, for fully 270° from the moonlet. Although this persistence is, in fact, not well understood and an area of ongoing study, we do not believe that the properties of the rings differ so greatly between the Encke Gap and the Cassini Division to allow wavy edges to persist 270° in one case and fully damp in less than 15° in another. Also, such rapid damping would remove the wake pattern which is itself the product of persistent orbital eccentricity of the ring material. With these arguments in mind, letting a = 118,288 km (the location of Edge 5) and a_s = 118,269 km, and using MT's *lower* limit estimate of $M_s/M_p = 10^{-11}$, we get an amplitude $ae \sim 46$ km. This is larger than the gap itself, which is a nonphysical situation. The narrow gap width would not be stable and would continue to widen. In fact, as noted earlier the size of the gap requires only a 2-km moonlet, which would be about 100 times less massive than the moonlet inferred from the RSS scan, assuming unit density. The associated wavelength of this wavy edge (from Eq. (2)) would be ~179 km, or ~0°.1, which would allow about 20 wavelengths to fit in the azimuthal range of the image while still being well above its resolution. If wave damping length is best measured in wavelengths and not in de-

grees, the Cassini Division wavy edges *may* damp in one-seventh of the azimuthal distance or ≈40° since the wavelength here of ~0°.1 is approximately equal to one-seventh of the wavelength observed on the Encke Gap edge, still a much greater distance than the inferred ~15° distance between FDS 43999.37 and the moonlet. Certainly, such a wavy edge would be visible in the image. Worse yet, if the image were leading the moonlet, as the moonlet wake model would suggest, then Edge 4 at a = 118,265 km would be perturbed even more strongly, having an absurd value of ae ~ 1000 km. Similarly, if the image FDS 43993.06 is leading (trailing) MT's inner moonlet we get ae ~ 13 km (11 km), while allowing about 70 wavelengths of λ ~ 0°.1 to fit on the image. Wavy edges of this amplitude and wavelength would be easily detected. As a comparison, edge waves found in the Encke Gap by Cuzzi and Scargle (1985) had an amplitude of ~2 km, which was visible in a Voyager image with a resolution comparable to that of image FDS 43999.37, with no computer enhancement required.

The six Voyager images used in this study were examined for edge waves of even smaller amplitude, following a procedure identical to that of Cuzzi and Scargle (1985). Azimuthal brightness scans were taken of Edges 1 through 10, the outer edge of the B Ring, and the edges of the Huygens Ringlet. These scans were obtained by radially averaging brightness values over an approximately two-pixel-wide scan parallel to the gap edge which resolved the entire frame into approximately 800 azimuthal bins. These scans were then spectrally analyzed by taking fast Fourier transforms to obtain any evidence of periodic features at relevant spatial frequencies. The spectra were studied carefully for the presence of signals above the noise level. Nothing was found which firmly established the presence of wavy edges; in fact nothing was found of strength comparable to the many detections of wavy edges in the Encke Gap by Cuzzi and Scargle (1985), some of which were invisible in Voyager images. A few signals of marginally detectable strength were found to be an effect of pixellation in the Voyager imaging system. This lack of wavy edges has two important implications. In the case of image FDS 43999.37, its location after precession at the corresponding orbital rate is near enough in longitude to the outer moonlet that, given the mass inferred from the RSS optical depth extrema, Eq. (3) implies that waviness should appear on any of Edges 2 through 5, with the strongest signal being on Edge 4 or Edge 5. None was found. Similarly, after precession at the inner moonlet rate, image FDS 43993.06 fell near enough to this moonlet that waviness could have been detected there as well. Again, none was found. In addition to the negative results of the wavy edge analysis of images FDS 43999.37 and FDS 43993.06, which lie closest to the predicted moonlet longitudes, the lack of wavy edges in any of the other images is inconsistent with an assertion that the structure found in Bands 1 and 2 in those images is related to any other similar moonlets, which would need to be correspondingly close in order to produce a wake pattern which matches the observed band structure. Again, we must conclude that the observations of regular structure in Bands 1 and 2 are simply not consistent with a moonlet wake interpretation.

3.3. Smaller Moonlets

The negative results of the analysis of the regular structure observed in Bands 1 and 2, while discouraging, certainly do not rule out the possibility that moonlets exist in the Cassini Division. It may be that we just are not looking closely enough. According to current theory (e.g., Lissauer *et al.* 1981, Henon 1981), the sizes of the gaps separating the four bands of the division suggest that any moonlets maintaining them could be about 2 orders of magnitude smaller in mass than moonlets inferred from the RSS optical depth extrema. Moonlets of this size (~2-km radius) would still produce sub-

stantial wake patterns, although the corresponding wavy edges would be only marginally detectable. That no evidence for such moonlets has been found may also be due to the small fraction of the circumference of the Cassini Division that has been observed at a sufficiently high resolution (~14%). Furthermore, whether or not even smaller moonlets might be capable of maintaining the many small gaps in the Cassini Division, they may still exist there and may play a role in the smaller-scale morphology of the division. Would such possibly more numerous, smaller moonlets be detectable? Assuming a gap width of 40 km, a moonlet orbiting in the center of the gap with a radius smaller than about 2 km would produce a wavy edge with an amplitude less than 1 km. Such a wavy edge would be marginally detectable at best even in the highest-resolution Voyager images of the Cassini Division and could account for the lack of wavy edges found in the images. However, chances are that a wake pattern of such a moonlet would be visible in the RSS scan, provided that the moonlet is close enough to the scan in longitude that the wavelengths of the wake pattern are greater than the radial resolution of the scan. Although the wavelength of a wake pattern increases with increasing radial distance from the moonlet, the amplitude of the wake simultaneously decreases. Recall that the MT moonlets are *not* in the gaps closest to the structure to which they are ascribed, but in fact must be one gap further away in order for the wake radial wavelength λ_r to be as large as observed. The large distance required for the MT moonlets, then, led to their large masses. For a minimal 2-km-radius body, it may be that at a great enough radial distance from the moonlet for the wavelength to be resolvable, the amplitude may decrease to the point at which the wake pattern is not detectable in the RSS scan. For a wake pattern to be resolvable by the RSS scan at, say, 5 km from the ring edge and 25 km from the moonlet, the scan would have to be less than 3° in longitude from the moonlet. The chance of the scan falling within a 6° range around a moonlet is, of course, less than 2%. However, the chance of falling within detectable range of a small moonlet would be significantly increased if there were a family of small moonlets orbiting in each 40-km gap.

The radio scan does reveal some regular optical depth fluctuations near the outer edge of Band 1 which consist of nine extrema with decreasing amplitude and increasing wavelength with increasing distance from the ring edge (Fig. 11). A comparison of this structure with the same region of the PPS scan indicates the likelihood for azimuthal variation, unlike the case with the larger-scale structure in Bands 1 and 2. Although the noise level of the PPS scan is high for the Cassini Division, this scan does indicate general trends in optical depth with relatively higher confidence. Figure 11 shows that the trend in optical depth within 20 km interior to Edge 2 is quite different for the two scans. The scale of the individual fluctuations observed in the RSS scan is less than 5 km and would not be resolved by the Voyager images used in this study, or addressed effectively by the PPS data, due to the high noise level at this smaller effective resolution.

The best fit of a moonlet wake model to this structure observed by the RSS scan near Edge 2 implies a small moonlet orbiting in the gap between Edges 2 and 3. To produce the observed structure, the moonlet would be trailing the RSS scan by $0.42 \pm 0.01°$ and would have an orbital radius of 118198.1 ± 0.3 km, or would be about 9 km away from Edge 2. The mass predicted for this moonlet is roughly $8.1 \pm 5.3 \times 10^{15}$ g or $1.4 \pm 0.9 \times 10^{-14}\ M_p$. Assuming a mass density of 1 g cm^{-3}, this mass translates to a moonlet radius of roughly ~1 km. The results of this analysis, following the approach of Showalter *et al.* (1986), are illustrated in Fig. 12.

Returning to the idea of a family of small embedded moonlets, how many moonlets, such as the one just described, would be

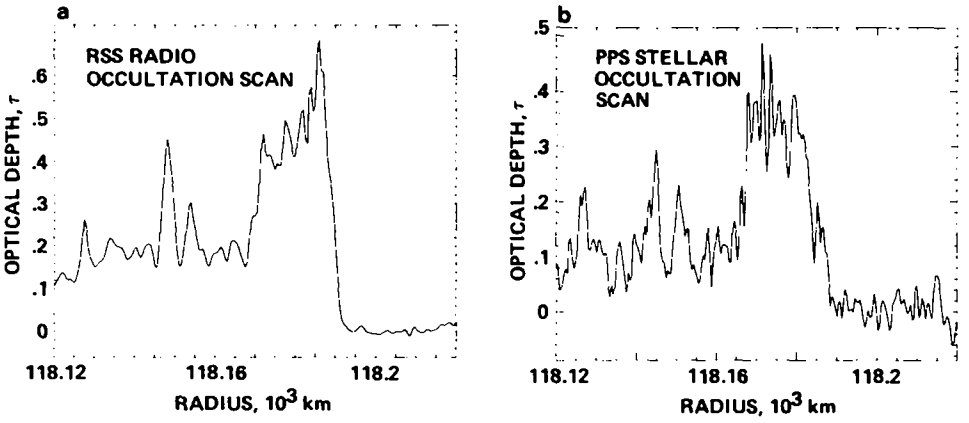

FIG. 11. (a) RSS scan of outer Band 1 showing regular structure from 118,170 km to Edge 2. (b) PPS scan of same region shown in (a).

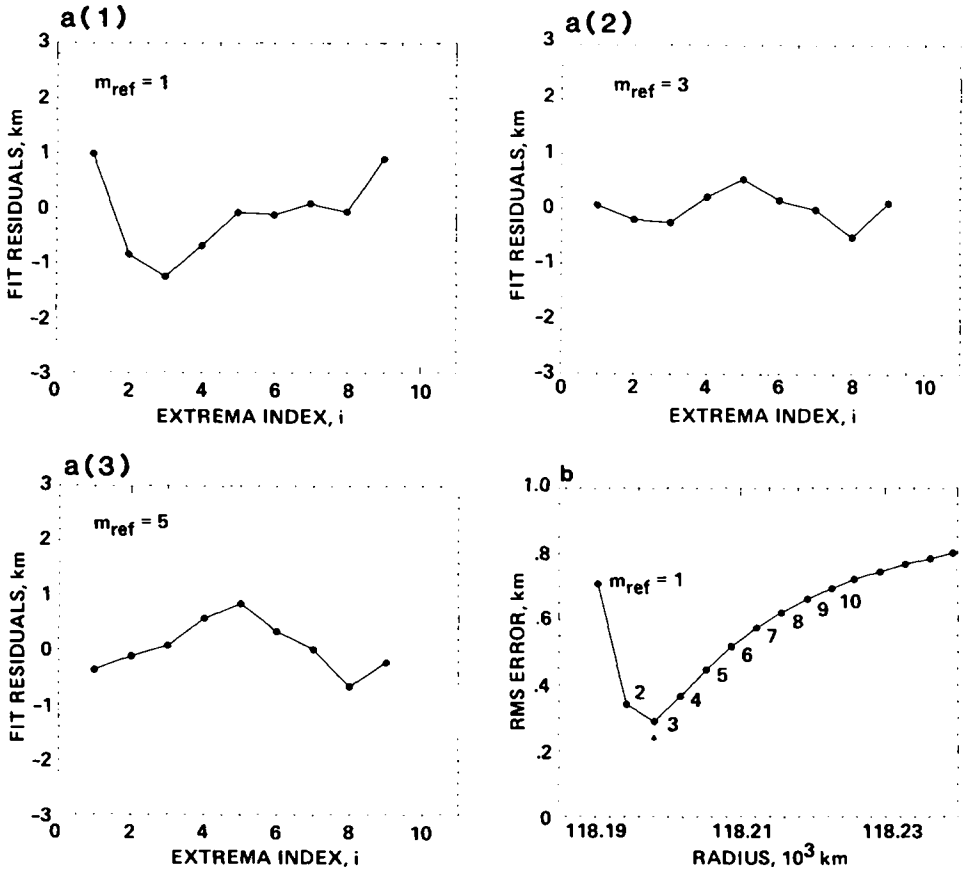

FIG. 12. (a) Results of wake model analysis of structure shown in Fig. 11a. following Showalter *et al.* 1986. The integer m_{ref} is a fitting parameter used when the starting index of the oscillations is not known. Note the flatness of the curve corresponding to $m_{ref} = 3$. (b) A minimum in RMS error is obtained for $m_{ref} = 3$, implying $a_s = 118{,}198$ km, and $\theta_s = 0°.4$.

required to maintain the 40-km gap between Edges 2 and 3? From Eq. (1), the size of the gap implies a mass of roughly 5×10^{16} g, or about 10 moonlets of the size estimated above. Such a population of moonlets would improve the probability that the RSS scan falls a mere fraction of a degree from one of them. With this number of moonlets, one might expect the RSS scan to detect more than just the wake of one moonlet. However, recalling that the wavelength of a wake pattern varies inversely with the azimuthal distance from the moonlet, increasing this distance by a factor of 3 to just over 1° would reduce the wavelengths of the wake pattern by the same factor, putting most of the wake below the 1-km resolution of the RSS scan, and making it undetectable. Of course, current work on sheperding theory (Goldreich and Porco 1987) suggests that this process is much more efficient than previously thought, thus requiring a smaller number of 1-km objects.

While the results of our analysis of this structure are intriguing, the evidence that the RSS scan provides is rather scanty and there is no confirming observation of the wake as is the case with the Encke Gap moonlet. It is mainly for these reasons that we cannot pursue this possible moonlet evidence any farther.

3.4. Elliptical Edges of Band 1

As was mentioned in Section 1, Edges 1 and 2 appear slightly eccentric in a composite of four Voyager 2 images of the Cassini Division (Fig. 1). In this section, we determine the eccentricities and orientations of these two edges by fitting sine waves to the edge locations and longitudes observed in the Voyager images, the RSS scan, and the PPS scan. To perform these fits, an appropriate first guess at the rate of precession of the edges must be made. Analysis by Porco (1983) of the nearly Huygens Ringlet found it to be mainly a simple Keplerian ellipse (azimuthal wavenumber $m = 1$) precessing at the rate due to Saturn's oblateness corresponding to $m = 1$ (free precession). The precession rate, or pattern speed, is in general,

$$\Omega_p = \Omega - \kappa/m, \tag{7}$$

where Ω is the orbital frequency and κ is the epicyclic frequency (Lissauer and Cuzzi 1982). Since the Huygens Ringlet is predominantly freely precessing, it is logical to explore whether Edges 1 and 2 are also freely precessing. The results of our fits are shown in Fig. 13. Edges 1 and 2 do seem to be well fit by simple $m = 1$ ellipses precessing at the free rate. In this context, the edges have eccentricities of order 10^{-5} and pericenters at 65° and 197° (in the EME50 coordinate system; see Showalter *et al.* 1986), respectively, at the epoch of the RSS scan. Although the edges of certain narrow, eccentric ringlets of Saturn and Uranus, which precess as rigid units, have been shown by Porco *et al.* (1987) to have small misalignments of their pericenters, or apsidal shifts, on the order of 1°, there is no evidence that Band 1 and its Edges 1 and 2 precess as a rigid unit. A fixed apsidal shift of ~132° would be much larger than any known at present, and it may be that the large difference in pericenter locations between Edges 1 and 2 is not fixed in time. However, assuming rigid free precession and using the free rate corresponding to the mean radius of Band 1 (118,064 km) provides $m = 1$ fits to Edges 1 and 2 which are essentially indistinguishable from the fits obtained above by assuming differential free precession, indicating that rigid precession cannot be ruled out for Band 1.

As a comparison to our results using the $m = 1$ free precession rate to fit Edges 1 and 2, we precess these edges at the rates corresponding to higher values of m. The fits obtained for a double lobed pattern ($m = 2$) are shown in Fig. 14. These fits, although not implausible, are substantially less reasonable than those for $m = 1$ and fits for higher values of m are even less defensible.

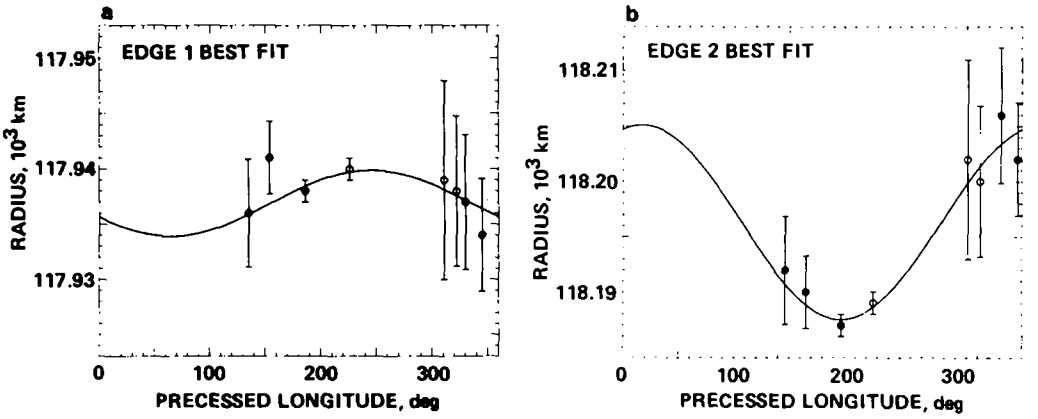

FIG. 13. (a) Sine wave fit of Edge 1 radii at longitudes precessed to the epoch of the RSS scan at the $m = 1$ free precession rate (5° day^{-1}) corresponding to the mean radius of Edge 1 (117,937 km). Best-fit values: mean radius a = 117,936.9 km, eccentricity e = 0.000025, and longitude of pericenter is 65°. (b) Sine wave fit of Edge 2 precessed at the free rate for Edge 2 (also very close to 5° day^{-1}). Best-fit values: a = 118,196.3 km, e = 0.000074, and longitude of pericenter is 197°.

3.5. Possible Explanations of Band 1 Structure

Although we believe that the larger-scale radial structure in Bands 1 and 2 is probably not related to embedded moonlets, the question of the true cause of this structure remains unanswered. It has been shown by MT that the two sets of optical depth fluctuations are not easily distinguishable from bending or density waves even though, they also note, the resonance locations predicted from the observed wavelengths do not correspond to those of any known exterior satellites.

Our own, similar analysis of the Band 1 extrema confirms the result of Marouf and Tyler regarding the RSS observation of Band 1 and provides very similar results for the four Voyager images which resolve all 13 extrema. For any steady disturbance of angular wavenumber m to be stabilized by

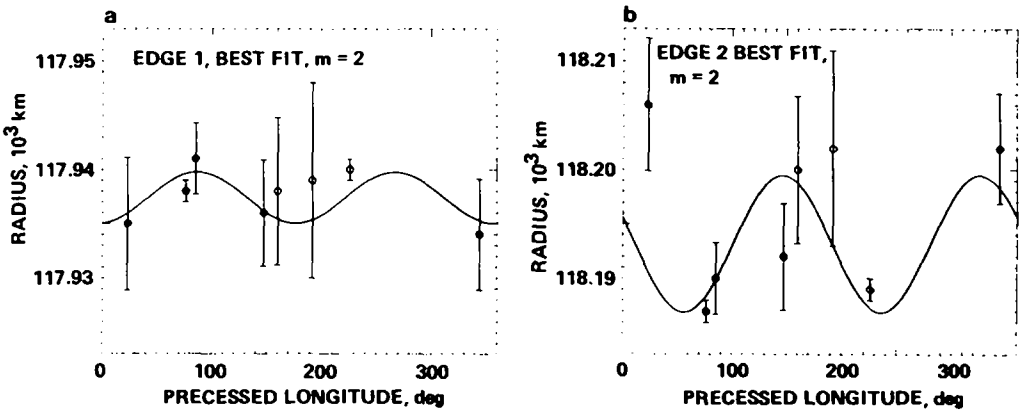

FIG. 14. (a) Sine wave fit of Edge 1 radii at longitudes precessed to the epoch of the RSS scan at the $m = 2$ free precession rate (379°5 day^{-1}) corresponding to the mean centerline radius of Band 1. Best-fit values: a = 117,937.4 km, and e = 0.000020. (b) Sine wave fit of Edge 2 precessed at the same rate as in (a). Best-fit values: a = 118,193.2 km, and e = 0.000053.

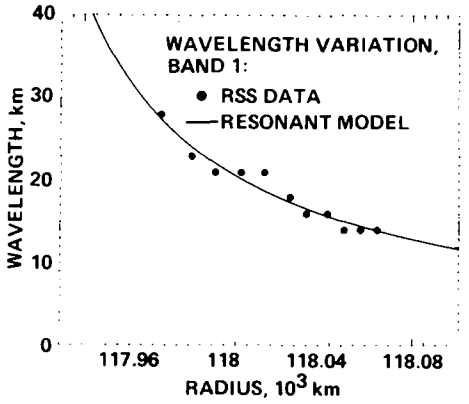

FIG. 15. Best fit of $\lambda = K(m, \Sigma, a)/(a - a_0)$ to Band 1 extrema observed in the RSS scan. Best-fit values of a_0, K, and RMS error can be found in Table III.

ring self-gravity, its pattern speed and radial wavelength are related functions of m. The relationships are determined from the dispersion relations most often associated with spiral density waves, but are of more general application. For example, we have used this dependence in Eq. (7) of Section 3.4 to calculate the rate at which to precess patterns of different m values. Similarly, we can fit a function of the form

$$\lambda = \frac{K(m, \Sigma, a)}{a - a_0} \qquad (8)$$

to the observed wavelengths, where $K(m, \Sigma, a)$, which is a weak function over the small range in a involved, takes on different forms depending on the value of m (discussed below), and a is the local radius. Such a fit allows the radius a_0 of resonance to be determined directly, and, if the azimuthal wavenumber m of the pattern is known, the local ring surface mass density Σ to be determined as well (Cuzzi *et al.* 1984). Our best fit of this sort is shown in Fig. 15.

The best-fit resonance locations resulting from this analysis (Table III) are closely distributed around the apoapse radius of the optically thick Huygens Ringlet (117,860 km). Therefore, we first explore a possible dynamical connection between the Huygens Ringlet and the structure in Band 1. Subsequently, we consider alternative dynamical causes of unknown origin.

The mainly $m = 1$ nature of the Huygens Ringlet location and pattern speed (Porco 1983), its good positional agreement with the location a_0 derived from the wavelength fits (Fig. 15), and the apparent $m = 1$ structure of Edges 1 and 2 suggest that it might be associated with an $m = 1$ perturbation on Band 1. Assuming that the Band 1 structure is the result of an $m = 1$ disturbance, we can calculate a value for the local surface mass density Σ from the observed wavelengths. For $m = 1$,

$$K(m, \Sigma, a) \approx \frac{8\pi^2 \Sigma a^6}{21 J_2 M_p R_p^2} \qquad (9)$$

(Cuzzi *et al.* 1984), and combining this with Eq. (8), we get

$$\Sigma = \frac{21 J_2 M_p R_p^2 \Delta a \lambda}{8\pi^2 a^6}, \qquad (10)$$

where J_2 is Saturn's second gravitational moment, M_p and R_p are Saturn's mass and equatorial radius, $\Delta a = a - a_0$ is the radial distance to the resonance location a_0, and λ and a are the local wavelength and radius.

TABLE III

PREDICTED RESONANCE LOCATIONS FOR BAND 1 STRUCTURE

Image (scan)	a_0[a] (km)	$K(m, \Sigma, a)$[b] (km²)	σ[c] (km)
34931.06	117,856.	2934.	3.1
34934.33	117,853.	3080.	1.5
43993.06	117,864.	2836.	3.5
43999.37	117,874.	2572.	2.3
RSS	117,878.	2610.	1.0

[a] Predicted resonance locations from fits of $\lambda = K(m, \Sigma, a)/a - a_0$ to observed values of (a, λ) in Band 1, where λ and a are the local wavelength and radius, respectively. The apoapse radius of the $m = 1$ component of Huygens Ringlet is 117,860 km (Porco *et al.* 1984).

[b] Fitting parameter. See Eqs. (9) and (11) for its definition.

[c] RMS error of each fit.

In this way, we obtain an average value $\Sigma \approx 0.94 \pm 0.06$ g cm^{-2} for Band 1.

If, on the other hand, we assume values of $m > 1$, we use the alternative form for $K(m, \Sigma, a)$ given by Cuzzi *et al.* (1984),

$$K(m, \Sigma, a) \approx \frac{4\pi^2 \Sigma a^4}{3(m-1)M_p}, \quad (11)$$

and, using our observed parameters, we obtain

$$\Sigma \approx \frac{3(m-1)M_p \Delta a \lambda}{4\pi^2 a^4} \sim 63(m-1) \text{ g cm}^{-2}. \quad (12)$$

Even for $m = 2$, the surface density would be considerably larger than values obtained in other regions of Saturn's rings which are also much more optically thick. In addition, one might expect such perturbations of larger m to also manifest themselves along Edges 1 and 2, contrary to our finding that Edges 1 and 2 are best fit by $m = 1$ ellipses.

For one comparison with the mass densities derived above, we use the following rough method of estimating a reasonable mass density for Band 1 based on a comparison of optical depth and statistically obtained particle size estimates for the inner and outer regions of the Cassini Division. Showalter and Nicholson (1988) calculate a particle size parameter Q for various radial regions of Saturn's rings which is proportional to the square of the "effective" (for likely size distributions, the largest) local particle size. Therefore, the change in effective particle size from one locality to another is $(Q_1/Q_2)^{1/2}$. Since particle mass is proportional to the cube of the largest typical particle size (assuming constant particle density), the change in particle size $(Q_1/Q_2)^{1/2}$ is also the change in particle mass per unit particle area. If we combine this factor with the total change in particle area from one radial location to another, which is just the ratio of optical depths τ_1/τ_2, then a rough estimate of the change in surface mass density can be obtained, given by

$$\Sigma_1 \sim \frac{\tau_1}{\tau_2}\left(\frac{Q_1}{Q_2}\right)^{1/2} \Sigma_2. \quad (13)$$

Scaling in this fashion from a value of $\Sigma \approx 10$ g cm^{-2} obtained from analysis of the Iapetus 1 : 0 resonance in the outer Cassini Division (Cuzzi *et al.* 1984), we obtain a value of $\Sigma \sim 5$ g cm^{-2} for Band 1, which is in much better agreement with our $m = 1$ value of $\Sigma \sim 1$ g cm^{-2} calculated from observations than with values of Σ for any higher value of m. Furthermore, a value of $\Sigma \sim 1$ g cm^{-2} is in the range of mass density values determined in regions of the C ring which have properties similar to those of the inner Cassini Division (Rosen and Lissauer 1988).

The above comparisons suggest that the value of surface mass density of Band 1 calculated for $m = 1$ is much more reasonable, supporting the case for an $m = 1$ disturbance possibly associated with the Huygens Ringlet and essentially ruling out any presently unknown resonances of higher m.

Another possibility is that the Band 1 optical depth fluctuations are not caused by a gravitational resonance, but are the result of the viscous stresses induced by neighboring particle streamlines on each other. Even in this process, the mass or optical depth fluctuations occur on a spatial scale determined by ring self-gravity; that is, they may be estimated with slight variations of Eqs. (10) and (12) above. This phenomenon, variously called "pulsational overstability" (Papaloizou and Lin 1988) or "dynamical instability" (Borderies *et al.* 1984, French *et al.* 1988, Goldreich and Porco 1987), has been shown to be capable of producing stable oscillations of various modes in rings considerably narrower than Band 1. However, in this case the resulting wavelengths would not be expected to vary systematically with radius, and we have shown that $\lambda \propto 1/(a - a_0)$ fits the observed wave pattern very well (Fig. 15).

Although the regular optical depth fluctuations in Band 1 seem best fit by an $m = 1$ density wave, the actual source of the dis-

turbance is not clear. As was noted previously, the predicted resonance location lies very near the apoapse radius of the Huygens Ringlet. Naively assuming this ringlet itself to be responsible for what is observed, one might expect to find a similar situation immediately surrounding the Maxwell Ringlet in the C Ring. Unfortunately, no similar structure is, in fact, found there in either images or the RSS scan. Consequently, we cannot firmly identify the ringlet itself as the cause of the Band 1 structure.

4. SUMMARY

Contrary to previous results, we find that the regular radial structure in Band 1, and perhaps that in Band 2 as well, is not due to embedded moonlets since it does not behave according to the wake theory used to infer the moonlets in the first place. First, the similarities in wavelength, radial location, and amplitude of the structure seen in the various observations suggest that they are all the same structure observed at different longitudes in the frame of any moonlet orbiting within either gap. When the image locations are precessed at rates corresponding to the orbits of the inferred moonlets, their resulting wide distribution in longitude suggests that the radial structures observed cannot be due to any two embedded moonlets. Second, even if we postulate that all the observations are quite close to their own, separate, responsible moonlets (each the same distance θ_s, from the observed wake; an unlikely coincidence), the theoretical variation in wavelength or position of the observed extrema is not seen across any of the frames. Third, no wavy edges have been detected in any of these images, even those of extremely high resolution. These observations, we feel, rule out the possibility that even an extremely ad hoc distribution of moonlets could be responsible for the Band 1 and 2 regular radial structure.

From examination of possible alternatives to the embedded moonlet hypothesis as the cause of the observed structure, we find evidence that the Band 1 structure, at least, may actually be a density wave-like disturbance. As described in detail in Sections 3.4 and 3.5, the $m = 1$ nature of Edges 1 and 2, the proximity of the inferred resonance location to the apoapse radius of the mainly $m = 1$ Huygens Ringlet, and the reasonable value of surface mass density (~ 1 g cm^{-2}) obtained only by assuming $m = 1$ suggest that the Band 1 structure could be due to $m = 1$ perturbations by the nearby Huygens Ringlet. However, because similar structure is not seen in the vicinity of the eccentric Maxwell Ringlet, a truly satisfactory explanation is elusive.

The second major result presented in this paper is the possible detection in the RSS scan of a wake-like feature which could be caused by a small ($\sim$1-km-radius) moonlet orbiting in the gap just exterior to Band 1. The best fit of a moonlet wake model to the observed optical depth extrema suggests an approximately 1-km-radius moonlet orbiting about 9 km outside Edge 2, and lagging the RSS scan by less than 1° of longitude. While such a moonlet would be about an order of magnitude too small in mass to maintain the $\sim$40-km gap in which it resides, it could possibly be only one of many such moonlets orbiting there. A family of moonlets would also make it more probable for the RSS scan to fall so close to one of them in longitude. A family of moonlets is merely one possible explanation for the existence of the gap since there is no further evidence in support of this hypothesis. However, we note that Cuzzi and Scargle (1985) pointed out one anomaly in an Encke Gap wavy edge that they suggested might be caused by a small moonlet, distinct from the major 10-km-radius object which dominates the gap. Also, the various kinks in the Encke Gap ringlet (and perhaps in R117909) might be easily ascribed to local perturbations by a tribe of otherwise undetectable kilometer-sized objects. Cuzzi and Burns (1988) have also discussed such a population in the vicinity of the F Ring.

ACKNOWLEDGMENTS

This research was supported by the Planetary Geology and Geophysics Program of NASA, and by the Voyager project. Brian Flynn's contribution to this work was done while he was an employee of IMI, Inc. We thank Luke Dones, Laurance Doyle, Doug Lin, Essam Marouf, Maureen Ockert, John Papaloizou, Paul Rosen, Jeff Scargle, Mark Showalter, Frank Shu, and Scott Tremaine for illuminating discussions, helpful suggestions, and critical comments.

REFERENCES

BORDERIES, N., P. GOLDREICH, AND S. TREMAINE 1984. Unsolved problems in planetary ring dynamics. In *Planetary Rings* (R. Greenberg and A. Brahic, Eds.), pp. 713–734. Univ. of Arizona Press, Tucson.

CUZZI, J., AND J. BURNS 1988. Charged particle depletion surrounding Saturn's F ring: Evidence for a moonlet belt? *Icarus* **74,** 284–324.

CUZZI, J., J. LISSAUER, L. ESPOSITO, J. HOLBERG, E. MAROUF, G. TYLER, AND A. BOISCHOT 1984. Saturn's rings: Properties and processes. In *Planetary Rings* (R. Greenberg and A. Brahic, Eds.), pp. 73–199. Univ. of Arizona Press, Tucson.

CUZZI, J., J. LISSAUER, AND F. SHU 1981. Density waves in Saturn's rings. *Nature* **292,** 703–707.

CUZZI, J., AND J. SCARGLE 1985. Wavy edges suggest moonlet in Encke's Gap. *Astrophys. J.* **292,** 276–290.

FRENCH, R., J. ELLIOT, L. FRENCH, J. KANGAS, K. MEECH, M. RESSLER, M. BUIE, J. FROGEL, J. HOLBERG, J. FUENSALIDA, AND M. JOY 1988. Uranian ring orbits from Earth-based and Voyager occultation observations. *Icarus* **73,** 349–378.

GOLDREICH, P., AND C. PORCO 1987. Shepherding of the Uranian rings. II. Dynamics. *Astron. J.* **93,** 730–737.

HÉNON, M. 1981. A simple model of Saturn's rings. *Nature* **292,** 33–35.

LANE, A., C. HORD, R. WEST, L. ESPOSITO, D. COFFEEN, M. SATO, K. SIMMONS, R. POMPHREY, AND R. MORRIS 1982. Photopolarimetry from Voyager 2: Preliminary results on Saturn, Titan, and the rings. *Science* **215,** 537–553.

LISSAUER, J., AND J. CUZZI 1982. Resonances in Saturn's rings. *Astron. J.* **87,** 1051–1058.

LISSAUER, J., F. SHU, AND J. CUZZI 1981. Moonlets in Saturn's rings? *Nature* **292,** 707–711.

MAROUF, E., AND G. TYLER 1986. Detection of two satellites in the Cassini division of Saturn's rings. *Nature* **323,** 31–35.

MAROUF, E., G. TYLER, AND P. ROSEN 1986. Profiling Saturn's rings by radio occultation. *Icarus* **68,** 120–166.

PAPALOIZOU, J., AND D. LIN 1988. On the pulsational overstability in narrowly confined viscous rings. *Astrophys. J.* **331,** 838–860.

PORCO, C. 1983. *Voyager Observations of Saturn's Rings*. Ph.D. dissertation, California Institute of Technology, Pasadena, CA.

PORCO, C., G. DANIELSON, P. GOLDREICH, J. HOLBERG, AND A. LANE 1984. Saturn's nonaxisymmetric ring edges at $1.95R_s$ and $2.27R_s$. *Icarus* **60,** 17–28.

PORCO, C., AND P. GOLDREICH 1987. Shepherding of the Uranian rings. I. Kinematics. *Astron. J.* **93,** 724–729.

PORCO, C., AND P. NICHOLSON 1987. Eccentric features in Saturn's outer C Ring. *Icarus* **72,** 437–467.

ROSEN, P., AND J. LISSAUER 1988. The Titan-1:0 nodal bending wave in Saturn's Ring C. *Science* **241,** 690–694.

SHOWALTER, M., J. CUZZI, E. MAROUF, AND L. ESPOSITO 1986. Satellite "wakes" and the orbit of the Encke Gap moonlet. *Icarus* **66,** 297–323.

SHOWALTER, M., AND P. NICHOLSON 1988. Saturn's rings through a microscope: Particle size constraints from the Voyager PPS scan. Submitted for publication.

SMITH, B., *et al.* 1982. A new look at the Saturn system: The Voyager 2 images. *Science* **215,** 504–537.

TYLER, G., E. MAROUF, R. SIMPSON, H. ZEBKER, AND V. ESHLEMAN 1983. The microwave opacity of Saturn's rings at wavelengths of 3.6 and 13 cm from Voyager 1 radio occultation. *Icarus* **54,** 160–188.

WIESEL, W. 1982. Saturn's rings: Resonance about an oblate planet. *Icarus* **51,** 149–154.